

# Cloud-Based Dynamic Programming for an Electric City Bus Energy Management Considering Real-Time Passenger Load Prediction

Junzhe Shi<sup>1</sup>, Bin Xu<sup>2\*</sup>, Xingyu Zhou<sup>3</sup>, Jun Hou<sup>4\*</sup>

1: University of California, Berkeley, Department of Civil and Environmental Engineering, 760 Davis Hall, Berkeley, CA 94720, USA.

2: Clemson University, Department of Automotive Engineering, 4 Research Dr., Greenville, SC, 29607, USA

3: University of Texas, Austin, Department of Mechanical Engineering, 204 E. Dean Keeton Street, Stop C2200 ETC II 5.160 Austin, TX, 78712, USA.

4: University of Michigan, Department of Electrical Engineering and Computer Science, 1301 Beal Avenue, Ann Arbor, MI, 48109, USA.

\* Corresponding author: Bin Xu, Clemson University, Department of Automotive Engineering, 4 Research Dr., Greenville, SC, 29607, USA. Phone: 864-626-8335, Email: xbin@clemson.edu. Jun Hou, University of Michigan, Department of Electrical Engineering and Computer Science, 221 Santa Clara Way, San Mateo, CA 94403, USA. Phone: 734-272-5516, Email: junhou@umich.edu.

**Abstract** - Electric city bus gains popularity in recent years for its low greenhouse gas emission, low noise level, etc. Different from a passenger car, the weight of a city bus varies significantly with different amounts of onboard passengers, which is not well studied in existing literature. This study proposes a passenger load prediction model using day-of-week, time-of-day, weather, temperatures, wind levels, and holiday information as inputs. The average model, Decision Tree, Gradient Boost Decision Tree, and Neural Networks models are compared in the passenger load prediction. The Gradient Boost Decision Tree model is selected due to its best accuracy and high stability. Given the predicted passenger load, dynamic programming algorithm determines the optimal power demand for supercapacitor and battery by optimizing the battery aging and energy usage in the cloud. Then rule extraction is conducted on dynamic programming results, and the rule is real-time loaded to onboard controllers of vehicles. The proposed cloud-based dynamic programming and rule extraction framework with the passenger load prediction shows 4% and 11% fewer bus operating costs in off-peak and peak hours, respectively. The operating cost by the proposed framework is less than 1% shy of the dynamic programming with the true passenger load information.

**Keywords:** Electric city bus, cloud computing, vehicle to infrastructure, dynamic programming, passenger load prediction

## 1. Introduction

Greenhouse gas emission by human activities has been dominating global warming since the mid-20th century [1]. Reducing carbon dioxide emissions by minimizing conventional fossil fuel applications is the key to the sustainable development for the whole world. US government plans to limit the carbon dioxide emissions of passenger cars to 88g/km in 2025 [2]. The electrified propulsion system [3], such as Hybrid electric vehicles (HEVs), plug-in hybrid electric vehicles (PHEVs), and all-electric vehicles (EVs), will replace conventional gasoline-power vehicles

in future markets. Due to their high passenger loading capacities [4], city buses are perfect for applying the techniques of electric vehicles to reduce carbon dioxide emissions. Besides, driving in a city involves a lot of braking and acceleration conditions [5]. The regeneration ability further improves the energy utilization rate of an electric bus because most of the kinetic energy can be charged back rather than becomes the heat loss in vehicle braking [6]. In addition, the application of electric city buses also leads to reductions in noise levels [7]. Because of the benefits electric buses bring, as of 2019, more than 425,000 electric buses have been deployed around the world [8].

Rather than only using batteries as the energy storage devices, other devices, including supercapacitors [9] and flywheels [10], are also widely used in transportation to minimize operational cost by extending the lifetime of batteries. Supercapacitors can be charged and discharged much more rapidly than conventional batteries without apparent aging [11]. However, using the supercapacitors as the only energy storage devices is not a good choice due to their low energy density. A supercapacitor can only store about 5 percent of the energy that lithium-ion batteries can store with the same weight [12]. Thus, one possible solution is to use a hybrid energy storage system (HESS) that has both advantages of supercapacitors and batteries, including high power density and high energy density.

An energy management strategy (EMS) plays a crucial role in a HESS because of the HESS complexity [13]. In the literature, various EMSs have been designed and discussed, such as the rule-based method, the Pontryagin Minimum Principle (PMP), Model predictive control (MPC), and Dynamic Programming (DP). A fuzzy-logic rule-based EMS is proposed for an electric bus [14]. The rule is offline optimized by DP. Even though DP is used, it is only optimized one time and does not consider the real-time load variation. Two rule-based EMSs, named Model Decision and Parallel driving Energy Management, are proposed for a series-parallel hybrid bus [15]. Energy consumption is reduced compared with an internal combustion power bus. However, the rule is fixed once it is developed and does not adaptive to real-time varying conditions. Different from rule-based methods, PMP, MPC and DP are optimization-based methods. A PMP based EMS is proposed for a plug-in hybrid electric bus on a fixed route [16]. The proposed PMP results show a close approximation to the offline DP results. However, the varying passenger load is not considered. In [17], an MPC with a Pareto-front analysis of the objective functions is used to reduce fuel consumption and battery degradation. However, the battery degradation rate is changing while batteries are aging, which is not considered. [18] utilizes the DP to deal with the integrated optimization for deriving energy split strategies of a hybrid electric city bus. Both MPC and DP are used in a plug-in hybrid electric [19]. Even though it has future operating condition prediction, its prediction accuracy is low. In addition, due to the high computational cost, DP is

only executed offline. Nevertheless, these papers neglect the passenger loading effect and assumes the city buses always keep the constant masses. Besides, these methods require a priori knowledge of driver power demand to specify the future power output of each actuator [20]. Once driving patterns are different from the designed one, the performances of the above methods cannot be guaranteed. Moreover, DP is only used offline due to the limited computation capability of the bus onboard controller.

To address the future passenger load prediction issue, collecting traffic information and predict future power demand become a potential way. Through Vehicle-to-Infrastructure (V2I) and Vehicle-to-Vehicle (V2V), communication holds a significant potential to improve the information acquisition for prediction of future traffic information [21]. A hierarchical EMS using vehicle-to-cloud connectivity and MPC on the vehicle side is recently discussed in [22]. However, applying MPC on the vehicle side with a short prediction horizon still leads to high computational costs. The rapid development of intelligent transportation systems (ITS) and widespread use of cloud computing offers excellent opportunities to improve the overall performance of energy management strategies [23]. Besides, vehicle-to-cloud (V2C) provides a chance to apply the accurate and optimal but high computation expensive prediction and control algorithms, store and process the massive amount of data, and update the structures and parameters of current algorithms. With the powerful cloud cluster, even the DP algorithm has the potential to execute in real-time. Overall, three research gaps are found in the existing researches:

- 1) Influence of the various passenger load for generating an optimal EMS of hybrid-electric buses is merely discussed,
- 2) The high computational cost of the vehicle onboard optimization-based EMS like MPC and DP, The V2I and V2V benefits are not fully explored in the perspective of EV EMS.
- 3) The lacking investigation on EMS optimization considering the change of battery degradation rate after batteries aged.

This paper extends the researches by discussing the effect of the passenger load factors and battery aging on the optimal EMS generation while proposing a new EMS to fill above three research gaps. The schematic diagram of using cloud data collection and computation for hybrid-electric buses is presented in Fig. 1. Due to several stochastic variables (e.g., weather conditions), a precise passenger load prediction is challenging [24]. This paper investigates the method of passenger load factor prediction using different statistic and machine learning models. With the assistance of V2C connect, the prediction of the reference power demand can be achieved by collecting the traffic

information and predicting passenger load factors. Then, the planning of the reference power splitting is obtained with the concept of “block MPC” on the cloud by dynamic programming method. In addition, a rule-based controller with rule update ability is designed to handle the error between the predicted and actual power demands on the vehicle side with the limited computational cost. In summary, the contributions of this study are as follows:

- 1) EV bus passenger load is predicted in real-time using all the available information like weather conditions, time-of-day, day-of-week, etc. As the on-board passenger number varies significantly during rush hours and off-peak hours, the passenger load prediction substantially increases the accuracy of power demand profile prediction for EV buses.
- 2) Four models are investigated for the passenger load prediction, including an average model and three supervised learning models. Due to the inputs (i.e., weather condition, time-of-day, day-of-week, etc.) are not highly connected, the supervised models shine in these complex modeling problems.
- 3) A cloud-based DP framework is proposed to take advantage of the V2I and V2C connectivity. The DP optimization is executed in the powerful cloud cluster, and then a rule-extraction procedure is followed to run the DP results in the low-cost CPU on the bus.
- 4) Battery degradation rate impacts on bus operation costs are analyzed.

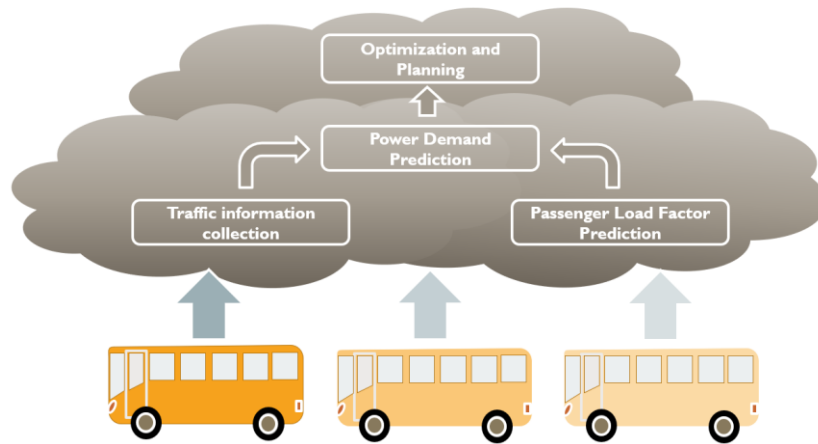


Figure. 1. The schematic diagram of cloud data collection and computation for hybrid-electric buses.

The remainder of this paper is organized as follows. Section II introduces the system modeling and configuration. Section III presents the passenger load prediction models. Section IV explains the three EMS utilized in this study. Section V first analyzes the aging effect and passenger loading effect, then presents the results of different passenger loading prediction models, and finally compares the three EMS. Section VII highlights the key conclusions of this paper.

## 2. Configuration and Modeling

In this section, the vehicle dynamics and system configurations of a hybrid electric city bus are presented. Besides, the models of battery and supercapacitor used in this study are discussed.

### 2.1 Vehicle Model and System Configurations

According to the specification of Mercedes-Benz eCitaro [25], the maximum energy capacity, maximum load capacity, and empty vehicle mass of the vehicle model are determined. The model aims to convert speed profiles to power demand profiles for the hybrid energy storage system based on different driving conditions. The vehicle dynamics can be expressed as,

$$m_{whole}gfv\cos(\alpha) + 0.5C_D A_f \rho v^3 + \frac{m_{whole}v dv}{dt} + m_{whole}gvsin(\alpha) = \begin{cases} P_{demand}\eta_T\eta_{md}, & P_{demand} > 0 \\ \frac{P_{demand}}{\eta_r}, & P_{demand} \leq 0 \end{cases} \quad (1)$$

$$m_{whole} = m_{vehicle} + m_{person}C_{max}f_{load} \quad (2)$$

where  $v$  is the vehicle speed,  $\alpha$  is the road slop,  $f_{load}$  is the passenger load factor, and rest of the parameters are summarized in Table 1.

Table 1  
Parameters and Description of the Electric City Bus.

Parameter	Description	Value
$m_{vehicle}$	Empty vehicle mass	13500 kg
$m_{person}$	Average mass of a person	70 kg
$C_{max}$	Maximum passenger load capacity	145
$E_{max}$	maximum energy capacity	293 kWh
$g$	Gravity acceleration	9.8 m/s <sup>2</sup>
$A_f$	Front area	7.5 m <sup>2</sup>
$f$	Rolling resistance coefficient	0.018
$C_D$	Air drag coefficient	0.7
$\rho$	Air density	1.29 kg/m <sup>3</sup>
$\eta_T$	Transmission efficiency	90%
$\eta_{md}$	Electrical machine efficiency	85%
$\eta_r$	Regenerative braking efficiency	65%

According to the required energy capacity of Mercedes-Benz eCitaro, the battery configuration is set up as 217 in series and 7 in parallel in this study. Besides supplying at least 15 seconds of peak power consumption, the supercapacitor pack is set up as 20 in series and 6 in parallel. The topology of the semi-active hybrid energy storage system is presented in Fig. 2. The electric motor drives the rear wheels. A DC/AC converter locates between the

electric motor and the two energy storage systems. A DC/DC converter is used to mitigate the voltage among battery, supercapacitor, and AC/DC converter.

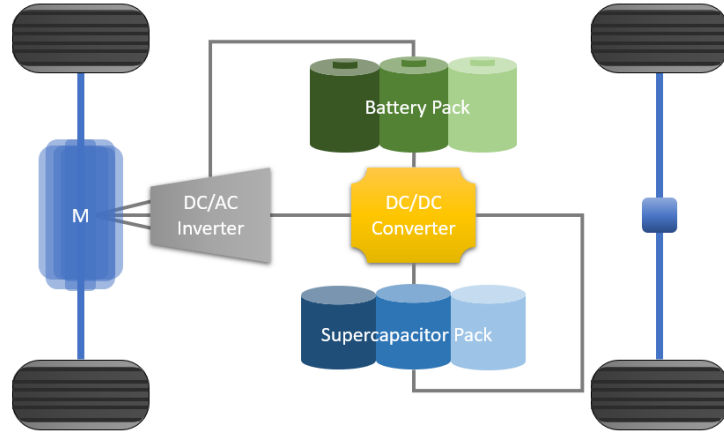
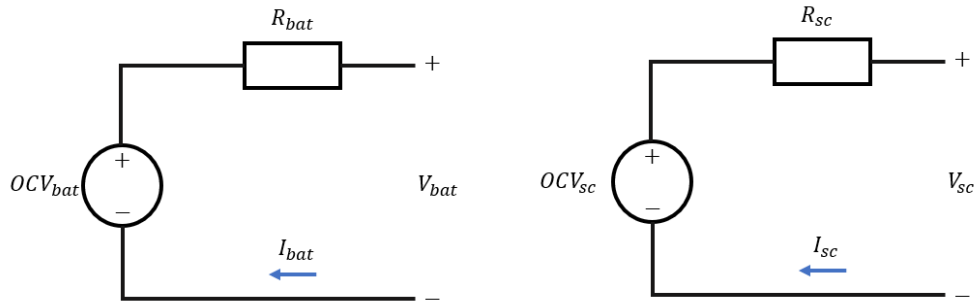


Figure. 2. Topology schematic of a semi-active hybrid energy storage system.



(a) Rint model of a battery

(b) RC model of a battery or a supercapacitor

Figure. 3. Simple equivalent circuit models of a battery and supercapacitor.

## 2.2 Battery Model

In this study, the state-of-charge (SOC) of a battery is defined as the state variables, while the current of the battery is defined as the control input. The dynamic of a battery is,

$$S\dot{O}C_{bat} = -\frac{I_{bat}}{3600Q_{bat}} \quad (3)$$

where the  $Q_{bat}$  is the nominal capacity of a battery.

As shown in Fig. 3 (a), the simple equivalent circuit model of a battery comprises an open-circuit voltage (OCV) and an ohmic resistor. The output and electric loss powers of a battery can be calculated by using,

$$P_{bat_{loss}} = I_{bat}^2 * R_{bat} \quad (4)$$

$$P_{bat_{output}} = OCV_{bat} * I_{bat} - I_{bat}^2 * R_{bat} \quad (5)$$

where,  $OCV_{bat}$  and  $R_{bat}$  are the OCV and the ohmic resistance of a battery. Their values depend on the  $SOC_{bat}$ , and the other parameters of the battery used in this study are listed in Table 2 [26].

Table 2  
Battery Parameters

Parameter	Value
Capacity (Ah)	60
Stored Energy (kWh)	0.192
SOC Usage Window (%)	10 - 90

The capacity of a battery limits the maximum energy of a battery that can supply. However, the capacity of a battery will fade while the battery is aging. Through cycling tests, an empiric aging model is obtained and verified in **Error! Reference source not found.** The capacity fade depends strongly on battery usage, C-rate, operating temperature, and depth-of-discharge. The battery depths-of-discharge (operating range) of a hybrid electric city bus is assumed from 90% to 10% SOC. The semi-empirical life model adopted the following equation to describe the correlation between the capacity loss, Ah throughput, temperature, and C-rate,

$$Q_{loss} = 0.0032 * \exp\left(-\frac{15162 - 1516 * C_{rate}}{RT_{bat}}\right) * Ah^{0.824} \quad (6)$$

where, the  $Q_{loss}$  represents the normalized capacity degradation,  $R$  is the gas constant which is equal to  $8.3145 \frac{J}{molK}$ ,  $T_{bat}$  is the absolute temperature of the battery, and  $Ah$  is the Ah throughput. After discretized the formula of the battery degradation equation (6), a dynamic degradation model is obtained,

$$\Delta Q_{loss} = \left(0.0032 * \exp\left(-\frac{15162 - 1516 * C_{rate}}{RT_{bat}}\right)\right)^{\frac{1}{0.824}} * Q_{loss}^{\frac{0.824-1}{0.824}} * 0.824 * \frac{\Delta t * I_{bat}}{3600} \quad (7)$$

where,  $\Delta t$  is the sampling time. While a battery is aging, the value of its resistance and capacity will change. In this study, the resistance and capacity of the batteries are assumed to be obtained and updated by online estimation.

### 2.3 Supercapacitor Model

As the same as a batterie, the SOC of a supercapacitor is also defined as the state variable, and the current of a supercapacitor is defined as the control input,

$$\dot{SOC}_{sc} = -\frac{I_{sc}}{C_{sc}V_{maxsc}} \quad (8)$$

where, the  $C_{sc}$  and  $V_{maxsc}$  are the capacitance and maximum voltage of a supercapacitor.

As shown in Fig. 3 (b), the Rint-Capacity model of a supercapacitor is comprised by an OCV and an ohmic resistor. The OCV of a supercapacitor is determined by,

$$OCV_{sc} = SOC_{sc} * V_{max\ sc} \quad (9)$$

The output and electric loss powers of a supercapacitor can be calculated by using,

$$P_{sc\ loss} = I_{sc}^2 * R_{sc} \quad (10)$$

$$P_{sc\ output} = OCV_{sc} * I_{sc} - I_{sc}^2 * R_{sc} \quad (11)$$

where,  $R_{sc}$  is the resistance, which depends on the C rate, and the other parameters of the supercapacitor used in this study are listed in Table 3 [26].

Table 3  
Supercapacitor Parameters

Parameter	Value
Max Voltage (V)	27
Capacity (F)	140
Stored Energy (kWh)	0.0142
SOC Usage Window (%)	50 -100

Unlike a batterie, a supercapacitor has a much longer cycle life, and its degradation is neglectable [27]. Therefore, the supercapacitor cycle life mode is not considered in this study.

### 3. Passenger Load Factor Prediction

A passenger load factor represents the capacity utilization of public transport services. 0% passenger load factor means the bus is empty, while a 100% passenger load factor means the bus is filled. This section focuses on the predictions of the passenger load factors using different models. Four models are discussed, including an average model and three regression models - Neural Network (NN), Regression Tree (RT), and Gradient Boosting Decision Tree (GBDT).

#### 3.1 Passenger Load Data Analysis

The actual passenger load data was collected from line 11 city buses in Guangdong, China. The raw data recodes the total number of people who took the line 11 city buses each hour from 08/01/2014 to 12/24/2014, as shown in the blue line of Fig. 4. There are four spikes regions at each month, which represents the weekdays busy hours of the four weeks. Each spike region has five lines, representing the five weekdays.



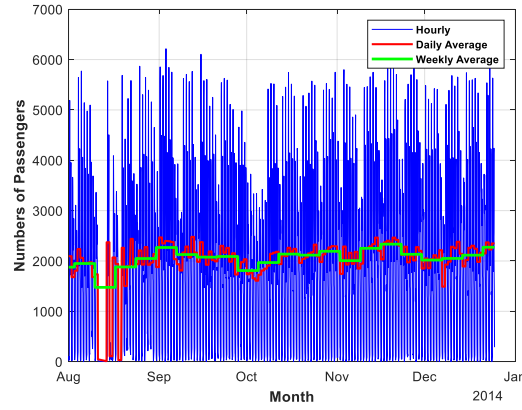


Figure. 4. The number of passengers who took the line 11 city buses in Guangdong from 08/01/2014 to 12/24/2014.

### 3.2 Average Model

The hourly, daily averages, and weekly averages of the passenger load data are also shown in Fig. 4. The pattern of daily average data is more regular than the weekly average data. Thus, the passenger load data is normalized and classified according to the day of a week, and shown in Fig. 5. In Fig. 5, the blue lines represented the passenger loads of a particular day, and the red lines indicate hourly average passenger loads of all weeks. Besides, the day-of-week data patterns can also work as the average model to predict the passenger load factors in the future.

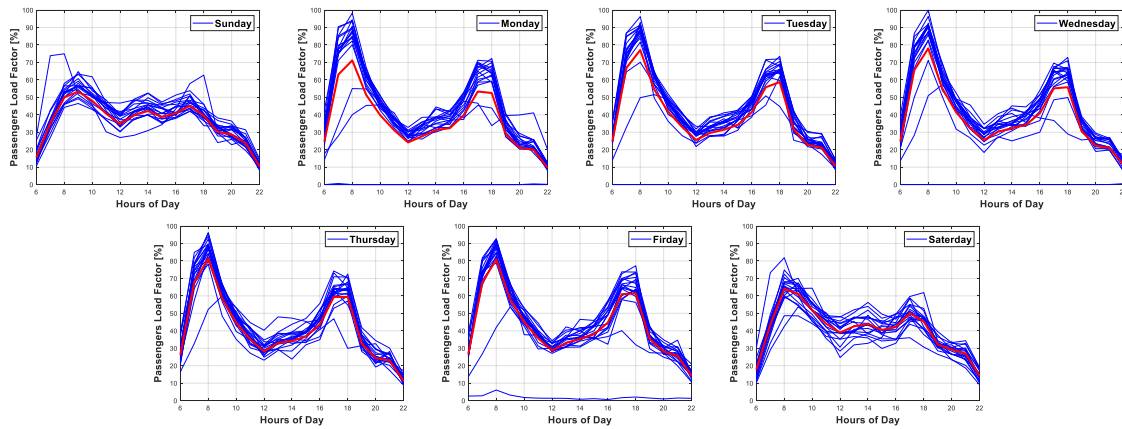


Figure. 5. Passengers load Factor from Monday to Sunday. Blue lines: passenger load of a particular day. The red line: hourly average passenger load of all weeks.

### 3.3 Regression Models

In this paper, the regression models, including Neural Network, Regression Tree, and Gradient Boosting Decision Tree, are considered and evaluated to increase the prediction accuracy of the average model. The inputs of these regression models are day-of-week, time-of-day, weathers, temperatures, wind levels, and holiday information. The

data of temperatures is presented in Fig. 6. The structures of each regression method are described in the following subsections.

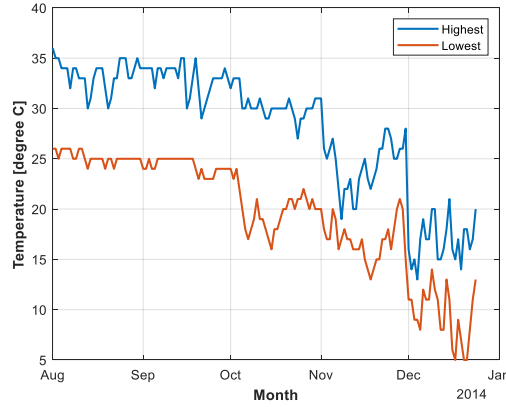


Figure. 6. The temperatures in Guangdong from 08/01/2014 to 12/24/2014. The blue line: the highest temperatures each day. The red line: the lowest temperatures each day.

### 3.3.1 Neural Network

Neural Networks (NN) are a class of statistical learning algorithms. Fig. 7. illustrates the structure of the four layers perceptron network used in the study.

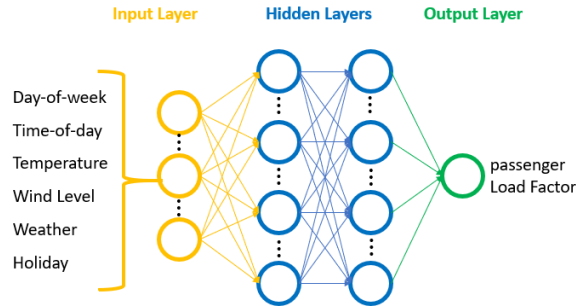


Figure. 7. Neural Network structure for the passenger load factor prediction.

The hidden layer performs nonlinear transforms for the feature extractions. Because the ReLu function provides fast calculation and converging speeds without a gradient vanishing issue, in the hidden layers, the ReLu function is selected as the activation function,

$$ReLU = \max(0, x) \quad (12)$$

For the neuron in the output layer, a linear activation function is applied,

$$Y = \theta^T a \quad (13)$$

During the training, the backpropagation algorithm is used to adjust the weights and thresholds of each neuron to minimize the error between the true passenger load factor and predicted results of the NN with current parameters sets up. In this paper, the NN is trained using gradient descent backpropagation for 200 epochs. For a further discussion of neural networks, readers can find more details in [28].

### 3.3.2 Regression Tree

Regression Tree (RT) is one type of decision tree and a machine learning method for predictions. Fig. 8. illustrates the structure of the Regression Tree used in the study. As a tree structure, the feature space of the RT is recursively partitioned into small parts to create its node and leaves. Once the splitting is completed, each leaf is fitted by a simple regression model.

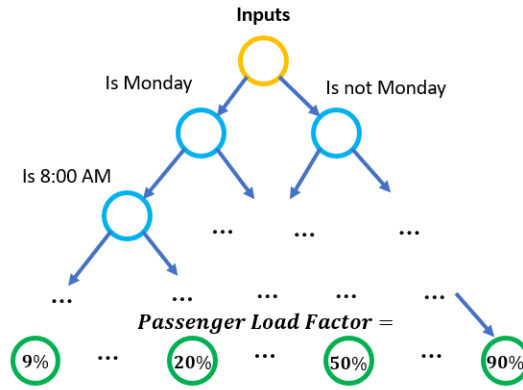


Figure. 8. Regression Tree structure for the passenger load factor prediction.

During the training process, the tree recursively splits a node (data set),  $S$ , into two child nodes (subsets),  $S_{Left}$  and  $S_{right}$ . By exhaustively searching over data space, the division  $\theta = (k, t_a)$ , composed of feature  $k$  and threshold  $t_a$ , is selected to minimize the total impurity of two child nodes. The forms of each child nodes are,

$$S_{Left}(\theta) = \{S | X_k \leq t_a\} \quad (14)$$

$$S_{right}(\theta) = \{S | X_k > t_a\} \quad (15)$$

In the paper, the impurity is defined as the sum of squared deviations between each passenger load factor data and the mean of all the passenger load factor variables in this branch,  $\bar{y}$ . For a branch with  $N$  variables, the impurity functions  $P$  is given by,

$$\bar{y} = \frac{1}{N} \sum_{i=1}^N y_i \quad (16)$$

$$P = \frac{1}{N} \sum_{i=1}^N (y_i - \bar{y})^2 \quad (17)$$

The training process stops after the relative decrease in the impurity is below a prespecified threshold, or the maximum tree depth is reached. For more discussions about a Classification and Regression Tree, more details can be found in [29].

### 3.3.3 Gradient Boosting Decision Tree

A Gradient Boosting Decision Tree (GBDT) uses an ensemble of decision tresses for predictions. During the training, a series of small decision trees are built. Each decision tree attempts to correct residuals from the previous one. The structure of the GBDT for the passenger load factor prediction is shown in Fig. 9.

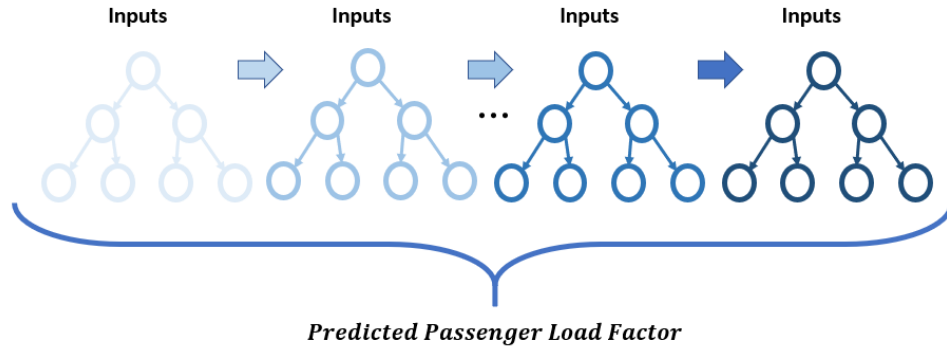


Figure. 9. The structure of Gradient Boosting Decision Tree for the passenger load factor prediction.

In this paper, the mean of the passenger load factors of the whole data set is selected as the baseline of the predictions. By comparing the predictions with actual data, residuals,  $r$ , can be calculated by the following equation,

$$r_i = y_i - \hat{y}(X_i) \quad (18)$$

where, the  $X$  is a set of inputs,  $y_i$  and  $\hat{y}(X)$  are the actual with the predicted data with given inputs. A decision tree with a shallow max depth can be constructed to predict the residuals based on the previous prediction results. With the additional decision tree, the prediction with inputs  $X$  are updated by the following the equation,

$$\hat{y}(X_i) = b + \alpha * DT(X_i) \quad (19)$$

where, the  $b$  is this baseline,  $\alpha$  is the learning rate that controls how hard each new tree tries to correct remaining residuals from the previous round, and  $DT(X)$  represents the predicted residual with given inputs. After prediction values are updated, residuals are calculated again to generate a new decision tree, which further improves prediction accuracy. The training processes repeat until the maximum numbers of decision trees are created. Once trained, all of the decision trees in the ensemble are used to make a final prediction by,

$$\hat{y}(X_i) = b + \sum_{m=1}^N \alpha * DT_m(X_i) \quad (20)$$

where,  $N$ , is total numbers of decision trees. Readers can find more details about the Gradient Boosting Decision in [30].

#### 4. Energy management strategies

This section introduces the three EMS utilized in this study. The structure of the three EMS is shown in Fig. 10. The first EMS is a standard offline dynamic programming strategy. All the future passenger load information is prior knowledge for dynamic programming. Due to the high computational cost of dynamic programming, the first EMS is only implemented in offline. The second EMS addresses the weakness of the high computational cost by extracting the rules from the offline dynamic programming results and implementing the rules in an online rule-based controller. However, this rule-based controller is not benefited from passenger load prediction. The third EMS is the proposed EMS framework by combining the advantages of the first EMS, second EMS, passenger load prediction model, V2I, and cloud computing. It takes advantage of the power cloud cluster to execute the dynamic programming using the predicted passenger load. The dynamic programming rule extraction is real-time conducted, and the rule is loaded to the onboard vehicle controller via the V2I connectivity. Detailed explanations of the three EMS are introduced in section 4.1, 4.1, and 4.3, respectively.

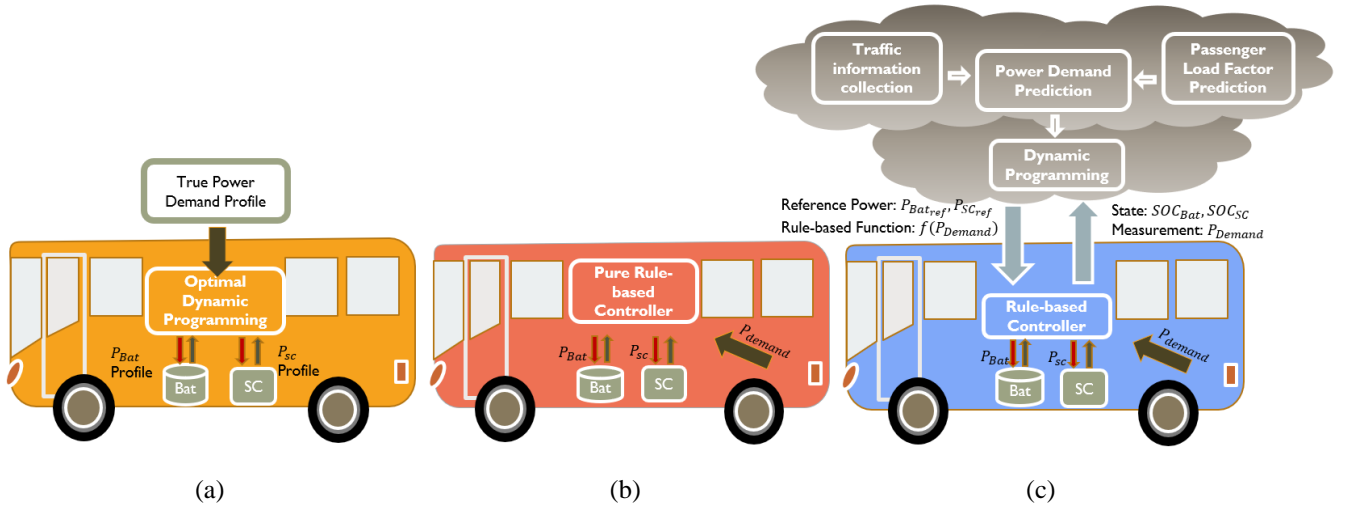


Figure. 10. Three EMS used in this study: (a) standard DP with true passenger load information, (b) rule-based controller with DP rule-extraction and no passenger load prediction, and (c) proposed cloud-based DP and rule-based controller with passenger load prediction.

#### 4.1 Dynamic Programming

First proposed by Richard Bellman in 1950s [31], the dynamic programming method breaks down a complex optimization problem into multiple subproblems, solves the subproblems, saves the solutions into a table, and then finds the solutions for the complex problem by looking up the table. The advantages of dynamic programming include: 1) Providing a globally optimal solution, 2) Designed for multi-stage decision processes, 3) Applicability of nonlinear systems, and 4) Handling of constraints.

The DP method is adopted in this paper to understand the minimum cost that a global optimization could bring to the entire driving cycle. In this study, the cost function of dynamic programming is formulated as follows:

$$J(k) = \sum_{t=k}^N (\Delta Q_{loss}(k) * P_{bat} + \Delta E_{loss}(k) * P_{ele} + W_{sc} * \sigma_{sc}(k) + W_{bat} * \sigma_{bat}(k)) \quad (21)$$

subject to the system dynamics:

$$SOC_{bat}(k+1) = SOC_{bat}(k) + \frac{-T_s I_{bat}(k)}{3600 Q_{bat}} \quad (22)$$

$$SOC_{sc}(k+1) = SOC_{sc}(k) + \frac{-T_s I_{sc}(k)}{V_{scMAX} C_{sc}} \quad (23)$$

and input constraints:

$$P_{demand}(k) = P_{bat}(k) + P_{sc}(k) \quad (24)$$

$$P_{bat}(k) = OCV_{bat}(k) I_{bat}(k) + R_{bat} I_{bat}(k)^2 \quad (25)$$

$$P_{sc}(k) = OCV_{sc}(k) I_{sc}(k) + R_{sc} I_{sc}(k)^2 \quad (26)$$

$$I_{scMIN} \leq I_{sc}(k) \leq I_{scMAX} \quad (27)$$

$$I_{batMIN} \leq I_{bat}(k) \leq I_{batMAX} \quad (28)$$

and state constraints:

$$SOC_{scmin} - \sigma_{sclow}(k) \leq SOC_{sc}(k) \leq SOC_{scmax} + \sigma_{schigh}(k) \quad (29)$$

$$SOC_{batmin} - \sigma_{batlow}(k) \leq SOC_{bat}(k) \leq SOC_{batmax} + \sigma_{bathigh}(k) \quad (30)$$

$$\sigma_{bat} \geq 0 \quad (31)$$

$$\sigma_{sc} \geq 0 \quad (32)$$

and cost constraints:

$$\Delta E_{loss}(k) = (I_{bat}(k)^2 * R_{bat_{ser}} + I_{sc}(k)^2 * R_{sc_{ser}}) * T_s \quad (33)$$

$$\Delta Q_{loss}(k) = \left( M * \exp\left(-\frac{Ea}{RT_{bat}}\right) \right)^{\frac{1}{z}} * Q_{loss}^{\frac{z-1}{z}}(k) * \frac{T_s * I_{bat}(k)}{3600} \quad (34)$$

where the sampling time  $T_s$  is 1 s, the price of battery capacity loss  $P_{bat}$  is 694.4 USD / Ah, and the price of electric  $P_{ele}$  is 0.1685 USD / kWh. To avoid the over-charging and over-discharging of batteries and supercapacitors, the operation windows of batteries and supercapacitors are constrained by 10% to 90% SOC of batteries and 50% to 99% SOC of supercapacitors.  $W_{sc}$  and  $W_{bat}$  weight the state constraints violations.  $\sigma_{sc}$  and  $\sigma_{bat}$  are the slack variables on the state constraints. When both constraints are met, and slack variables  $\sigma_{sc}$  and  $\sigma_{bat}$  are zero in the optimal solution. However, if constraints are violated, softened state constraints ensure the feasibility of the problem, and their associated linear weights can immediately penalize small constraint violations.  $J(k)$  indicates the accumulative cost of the capacity loss of batteries and electric loss of resistances from time N to time k. According to Bellman's cost-to-go principle, by solving the DP backward, the minimal costs of all states along the entire driving cycle can be found and stored as a global optimal control strategy.

#### 4.2 Rule-based Controller with Rule Extraction from Dynamic Programming

The rule-based method is one of the most widely used energy management strategies to split power between batteries and supercapacitors at different conditions. When the demand powers are high, the supercapacitors are used to supply the powers to avoid the degradation of batteries. However, supercapacitors cannot keep a high-power supply for a long time because of their relatively low energy density. The supercapacitors should be charged by regeneration power or batteries to keep the power supply ability for the future. Thus, the critical point of designing a rule-based controller is to figure out the charging and discharging conditions of the supercapacitors. The results of an offline DP are usually used to generate an optimal rule-based controller. By plotting one of the DP results in Fig. 11, we can see that the relationship between the power demands and supply powers of supercapacitors is almost linear. Because the DP provides globally optimal results, by fitting the relationship between the power demand and supply power of supercapacitors with the linear regression method, an optimal rule of the rule-based controller can be obtained.

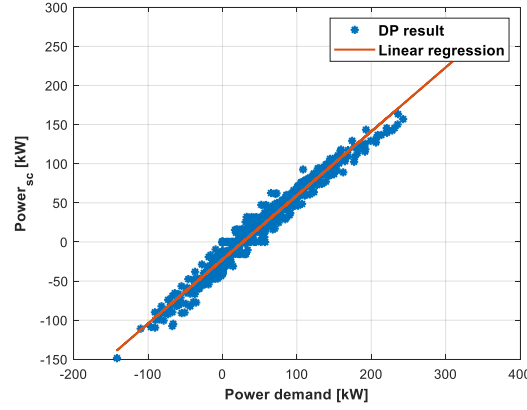


Figure. 11. DP result of  $P_{sc}$  vs.  $P_{demand}$  with 100 % passenger load factor.

Due to the lack of future power profile information, to avoid the over-charged and over-discharge of the supercapacitors, 1% SOC buffer zones are set for the lower and higher bounds of the supercapacitor SOC operation range. The flow chart of the rule-based controller is presented in Fig. 12. Supercapacitor only uses the extracted rule from DP when  $SOC_{SC}$  is in the range of 51%-99%.

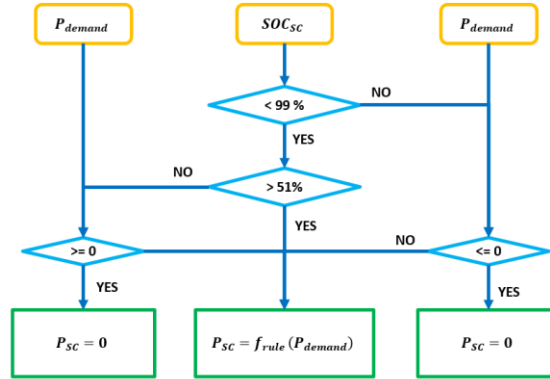


Figure. 12. The flow chart of the rule-based control that extracted from DP results.

#### 4.3 Cloud-based Dynamic Programming with Passenger Load Prediction

The rapid developments of cloud computation and telecommunication technologies provide the potentials to apply high computational cost but optimal algorithms for real-time applications. With cloud assisting, real-time traffic information can be collected, and the algorithm mentioned in the previous section about the city bus passenger load factors prediction can be implemented. In this subsection, an innovative energy management strategy, combining dynamic programming via cloud computing and rule-based controller with the rule update, is proposed for hybrid-electric buses. The structure of the proposed method is demonstrated in Fig. 10 (c).



The power demands are predicted by collecting traffic information and predicting passenger load factors on the cloud side. A discrete-time DP is applied to generate reference power profiles of batteries and supercapacitors and the rule of the rule-based controller with predicted power demands. The prediction horizon of the DP is set as 1200 seconds, and the DP is performed every 60 seconds with updated current states of the batteries and supercapacitors. Namely, the DP works as a block model predictive controller that generates optimal reference control signals with a long prediction horizon and allows the local controllers to follow the first 5% of the reference control signals. The prediction horizon and update frequency are design parameters determined by the trade-off between computational cost and performances. With accurate models and predicted power demands, a longer prediction horizon and faster update frequency provide better performances but lead to higher computational costs.

Due to the disturbances and the predictive errors of passenger load factors and traffic information, the actual power demands may differ from the reference power demand used in cloud DP. Thus, on the vehicle side, the rule-based controller is used to handle the errors between the actual and reference power demands by the following equations,

$$P_{demand_{ref}} = P_{sc_{ref}} + P_{bat_{ref}} \quad (35)$$

$$P_{sc} = P_{sc_{ref}} + \left( f_{rule}(P_{demand}) - f_{rule}(P_{demand_{ref}}) \right) \quad (36)$$

$$P_{bat} = P_{demand} - P_{sc} \quad (37)$$

where,  $P_{sc_{ref}}$  and  $P_{bat_{ref}}$  are the reference powers of batteries and supercapacitors from the cloud DP,  $P_{demand_{ref}}$  and  $P_{demand}$  are the reference and actual power demand,  $P_{sc}$  and  $P_{bat}$  are the actual powers supplied from batteries and supercapacitors, and  $f_{rule}$  is the optimal rule of a rule-based controller is updated by the optimization results of the cloud DP.

## 5. Results Analysis

In this study, real-time energy management strategies are tested and validated by the typical China Bus Driving Cycle (CBDC). The CBDC speed profile was converted to different power demand profiles with different passenger load conditions. The CBDC speed profile and power profiles with different passenger load factors are presented in Fig. 13. The CBDC speed profile shows frequent acceleration and braking events with the maximum speed below 15m/s (i.e., 53km/h or 33mph). Power demand varies significantly along with different passenger load factor as the 100% load factors results in high peaks at high speed and deep valleys at braking.

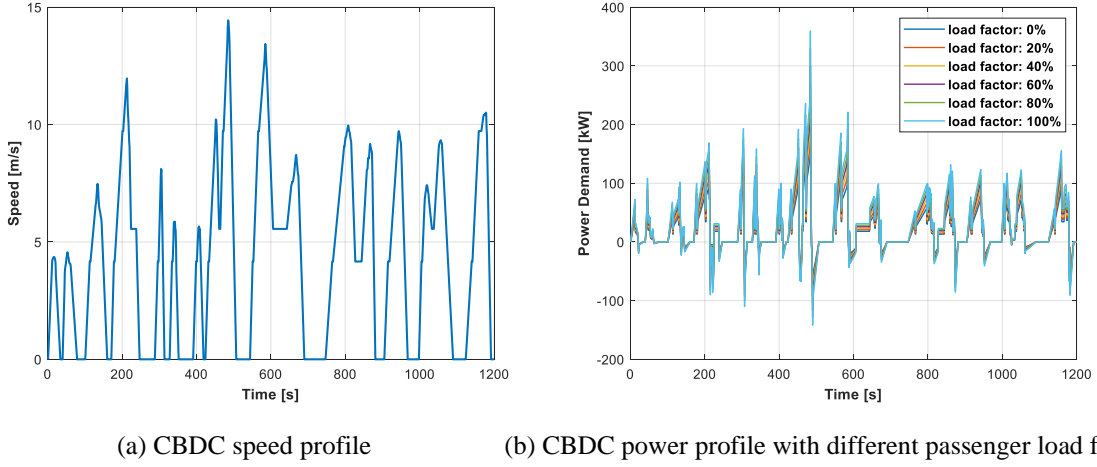


Figure. 13. China Bus Driving Cycle

### 5.1 Aging Effect

In order to analyze the impact factors of an optimal energy management strategy generation of hybrid city buses, a comparison study is performed in this subsection. The dynamic programming approach was utilized as the energy management strategy in the battery aging effect discussion.

Based on Eq. (7), the delta capacity loss in a sample time depends on the battery temperature, C-rate, and previous accumulated battery capacity loss. As shown in Fig. 14, with fixed battery temperature and crate, the delta capacity loss of a battery in a sampling time decreases while the battery is aging (i.e., y-axis drops as state-of-health (SOH) decreases from 100% to 50%). SOH = 100% corresponds to a brand-new battery and SOH = 0 % means 20% capacity loss, as known as end-of-life (EOL). Namely, the cost of battery capacity loss in a sampling time will decrease progressively as the batteries aged at the same operating conditions. In addition, using batteries to charge supercapacitors leads to extra electrical costs because of the electrical energy losses due to the resistances of supercapacitors. Thus, one thing that can be expected is that the battery aging effect impacts the formulation of optimal energy management strategy. If the state-of-health of the batteries is low, the optimization algorithm (21) will put more effort into minimizing the electric loss rather than the battery degradation loss.

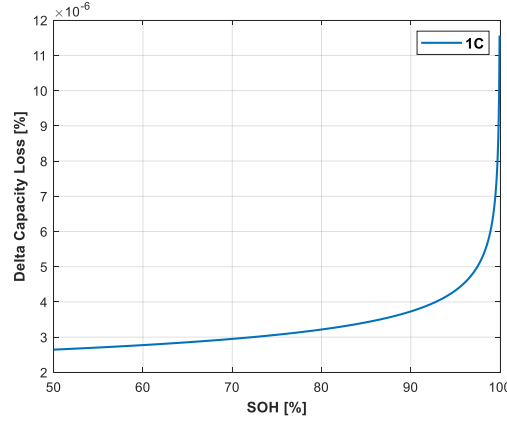


Figure. 14. The delta capacity loss of a battery with 1 C discharge current from 100 % SOH to 50% SOH.

To further validate and analyze the aging effect of the batteries on the optimal energy management strategy generation, the control strategies that consider the aging effect have been tested in this study. The dynamic programming generates two control strategies with the same power profiles but different battery SOH values. Then, these two control strategies are tested by the same vehicle operating condition. The results are shown in Fig. 15.

As shown in Fig. 15, the strategy (Strategy 1) represented by the blue line is generated with a 100 % passenger load factor and 100 % SOH. The strategy (Strategy 2) showed by the red line came from the 100% passenger load factor and 0 % SOH. In the test, both strategies were tested by an operation condition with a 100 % load factor and 100 % battery SOH. The total costs of Strategy 1 and strategy 2 are 3.8573 USD and 3.8795 USD, respectively. The result means that the correct SOH strategy only brings 0.58% of improvement than the strategy generated with a wrong SOH value. Namely, in this test, the SOH does not play an important role in the optimal control strategy generation. The result is surprising as we would expect larger improvement with correct SOH estimation.

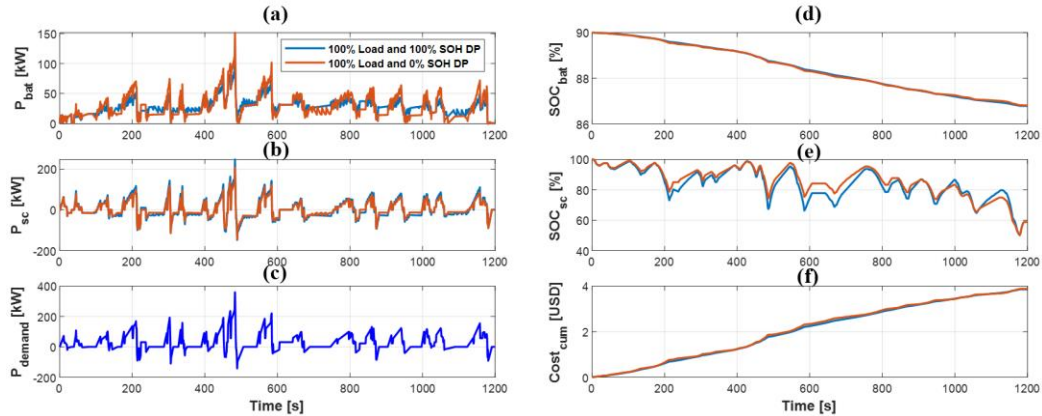


Figure. 15. Aging effect comparisons of 100% SOH and 0% SOH DP strategies by using a 100% SOH operation condition: (a) power profiles of batteries, (b) power profiles of supercapacitors, (c) power demand profile, (d) SOC profiles of batteries, (e) SOC profiles of supercapacitors, and (f) total cumulated cost.

To further investigate the logic behind the result, the costs along the CBDC using the same control strategy with 100% and 0% SOH are plotted and shown in Fig. 16. As shown in Fig. 16, the real-time cost of capacity loss with 0% SOH is much less than the cost with 100% SOH. The result matches the expectation. However, although the cost of battery capacity loss drops a lot from 100% SOH to 0% SOH, the real-time cost is still much higher than electrical loss. Namely, during the optimization, more efforts were put on minimizing the cost of the capacity loss rather than the electrical loss due to the resistance in both cases. As a result, similar control strategies were gained even they generated from different SOH conditions. In conclusion, the SOH of a battery would not significantly impact the optimal energy split strategy generation in the studied vehicle unless the manufacture cost the Li-ion batteries substantially decrease or electricity price increases in the future.

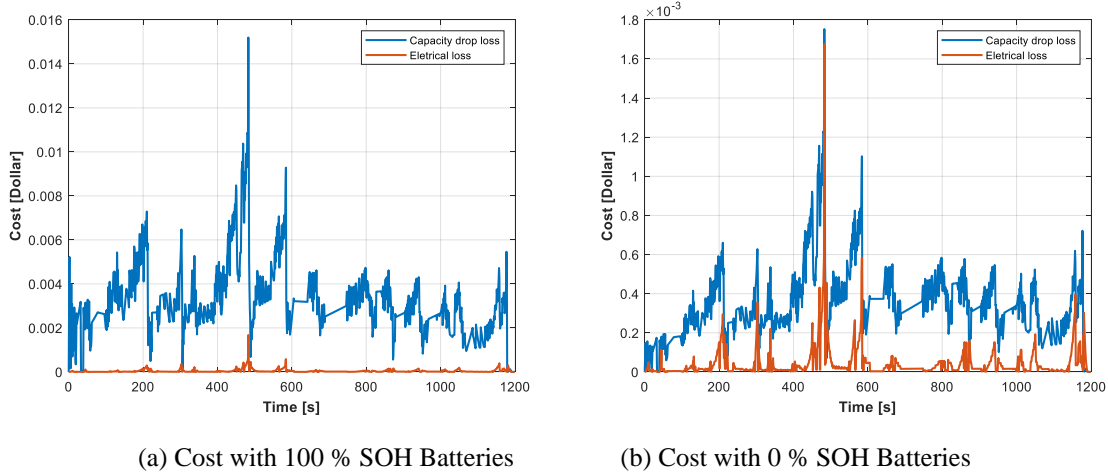


Figure. 16. Real-time cost comparison with different SOH of Batteries.

## 5.2 Passenger Loading Effect

As shown in Fig. 13 (b), a higher load factor leads to higher power demands. Simultaneously, the higher power demands require higher C-rates that batteries and supercapacitors have to supply. As shown in Fig. 17, the battery capacity loss cost increases exponentially as the C-rate increases. Thus, as the passenger load factor increasing, more control efforts should be put on avoiding charging or discharging batteries with high C-rates to minimize the battery capacity loss.

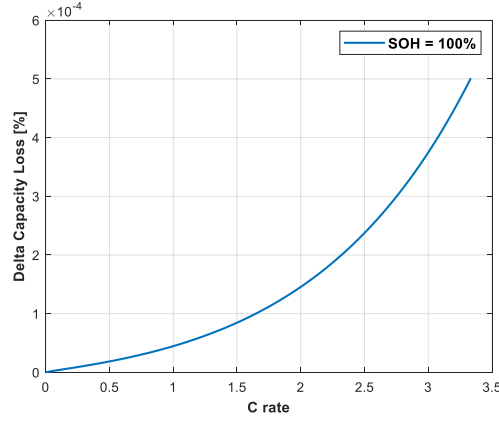


Figure. 17. The delta capacity loss of a battery with 1 C to 3.5 C discharge current and 100 % SOH.

Two control strategies are generated based on 100% load (Strategy 1) and 0% load (Strategy 2), respectively, with the dynamic programming algorithm to investigate the effect of the passenger load factor. These two control strategies were then tested with a 100 % load and 100 % battery SOH condition. As shown in Fig. 18, there is a large difference between the two strategies. When power demands are low, Strategy 1 is more likely to charge or save the energy of supercapacitors than Strategy 2. By keeping high SOC values of supercapacitors during low power demand range, Strategy 1 lets supercapacitors to provide more power supply than batteries when power demands are high. As a result, the total costs of Strategy 1 and strategy 2 are 3.8573 USD and 4.1369 USD, respectively. Without considering the loading effect, Strategy 2 introduced 7.24 % more cost than Strategy 1. This large percentage difference caused by the different passenger loading effect indicates the importance of the loading effect. It means that the passenger load factor should be considered while designing an optimal energy control strategy.

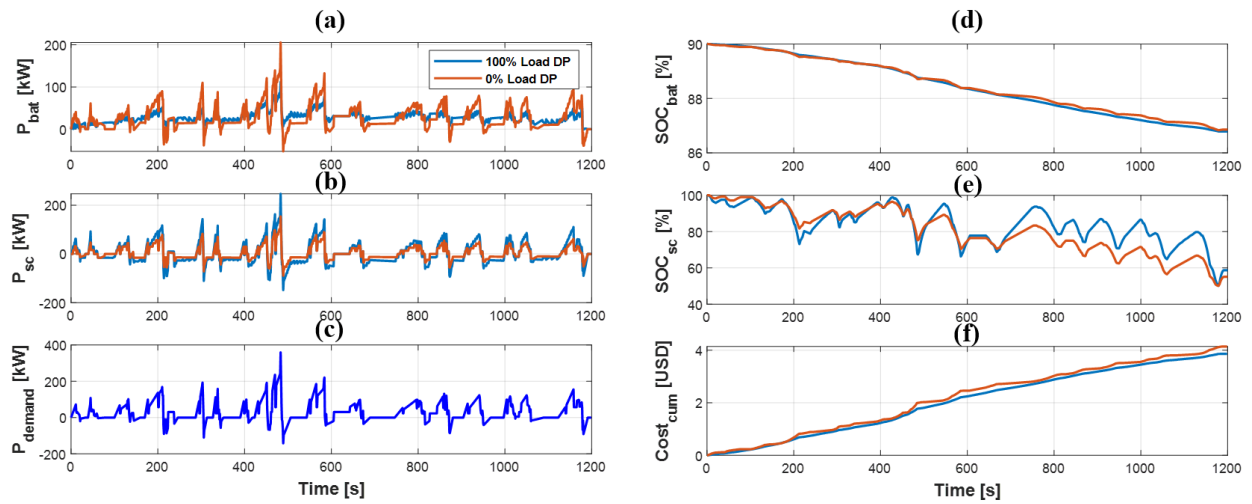


Figure. 18. Loading effect comparisons of 100 % load and 0% load DP strategies basing on CBDC and 100 % load factor: (a) power profiles of batteries, (b) power profiles of supercapacitors, (c) power demand profile, (d) SOC profiles of batteries, (e) SOC profiles of supercapacitors, and (f) total cumulated cost.

Besides, by extracting rules from DP, the fitted functions with CBDC and different passenger load factors are shown in Table 4 to demonstrate the impacts of passenger load factors on the rule update of rule-based controllers. The function in each row is fitted using the DP results considering the specific passenger load factor from that row.

Table 4

The rule of rule-based controller with different passenger load factors.

Passenger Load Factor (%)	Fitted Function (W)
0	$P_{sc} = 0.8391 * P_{demand} - 11803$
20	$P_{sc} = 0.8277 * P_{demand} - 13808$
40	$P_{sc} = 0.8270 * P_{demand} - 15948$
60	$P_{sc} = 0.8268 * P_{demand} - 18247$
80	$P_{sc} = 0.8240 * P_{demand} - 20402$
100	$P_{sc} = 0.8183 * P_{demand} - 22476$

As shown in Table 4, with a higher passenger load factor, the slop and intercept value of a fitted function are smaller. Because a higher passenger load factor leads to high power demands, supercapacitors need to supply more power at the high-power demand ranges to minimize the capacity loss of batteries. The optimization results tend to charge supercapacitors with more powers or save the energy of supercapacitors when power demands are low. Thus, for proposed EMS, with the updated rule of the rule-base controller at different passenger load conditions, the error between predicted and true power demands can be handled in an optimal way.

### 5.3 Passenger Load Factor Prediction

The average and regression models are trained using the Guangdong line 11 city buses passenger load data sets from 08/01/2014 to 12/14/2014. In the subsection, these models are tested by one-week passenger load data from 12/15/2014 to 12/22/2014. From the test, the comparisons between actual and predicted passenger load factors of each model are presented in Fig. 19. Among the four models, RT and GBDT prediction results show good alignment with the true results. NN model has extremely good prediction accuracy on all the days except Dec 16 and 17. The average model underestimates nearly all the peak load factors.

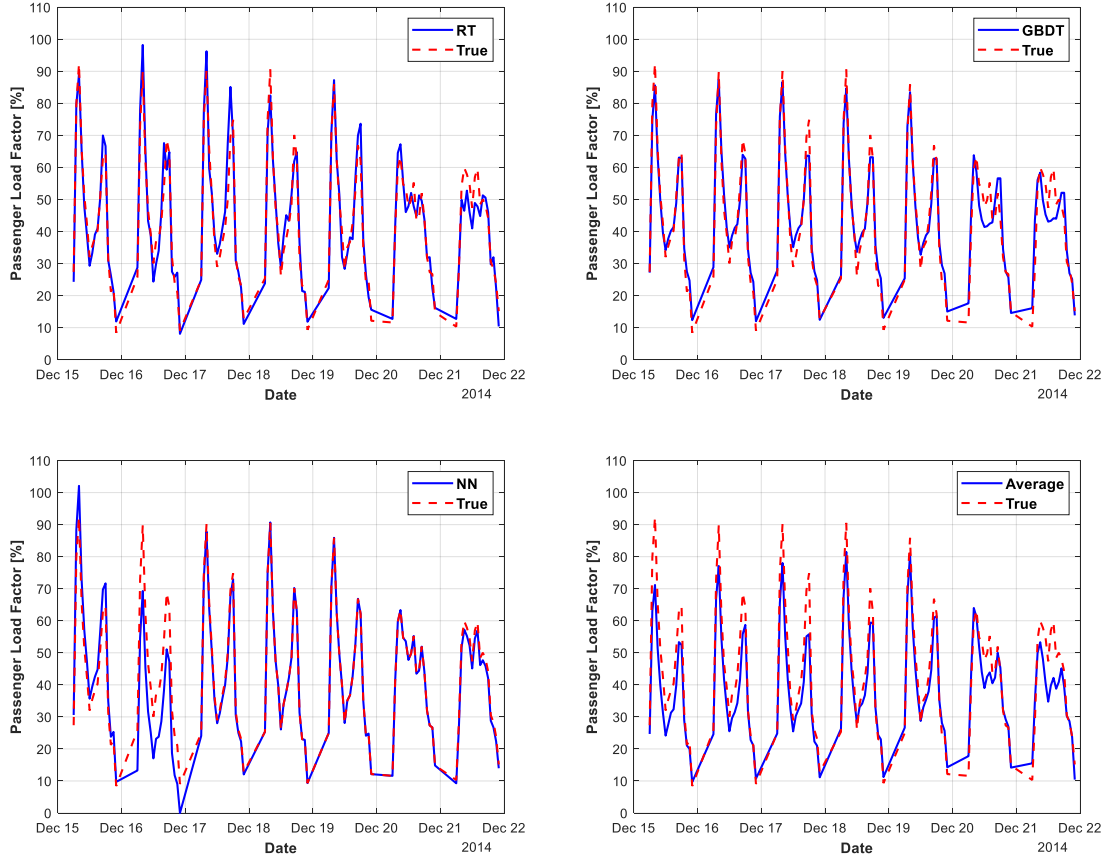


Figure. 19. Passenger load factor prediction test for RT, GBDT, NN, and Average models with one-week Guangdong line 11 city bus passenger load data from 12/15/2014 to 12/22/2014.

To further analysis the accuracies of prediction results, the accuracy of the forecast is evaluated by the root mean squared error (RMSE),

$$RMSE = \sqrt{\frac{1}{m} \sum_{i=1}^m (y_i - \hat{y}_i)^2} \quad (38)$$

where  $y$  and  $\hat{y}$  are the true and predicted passenger load factor, and  $m$  represents the number of the predictions. RMSE of each day and the whole week for each model are calculated and presented in Table 5. Besides, the variance of these RMSE of each model in the whole week are gained by using,

$$V = \frac{1}{N-1} \sum_{i=1}^N |RMSE_i - \overline{RMSE}|^2 \quad (39)$$

where,  $N$  is the numbers of day in a week, and  $\overline{RMSE}$  is the mean RMSE of each model.

Table 5

The RMSE of each day and the whole week for each model.

<b>RSME Model</b>	<b>Mon</b>	<b>Tu</b>	<b>Wed</b>	<b>Th</b>	<b>Fri</b>	<b>Sat</b>	<b>Sun</b>	<b>Total</b>	<b>Variance</b>
RT	3.0113	5.7436	6.6337	4.2158	4.2971	3.8723	6.0119	4.9776	1.7285
GBDT	3.2303	3.2929	4.2915	3.6366	2.7078	6.5581	7.6120	4.7988	3.4977
NN	5.4844	14.9115	1.3670	0.0665	0.0091	0.0017	2.1439	6.0816	29.4542
Average	10.3139	7.1619	8.5135	4.7929	3.7301	5.1463	9.1172	7.3353	6.1290

As shown in Table 5, the three regression models all work very well. NN model provides very accurate predictions from Wednesday to Sunday. The performances of the RT model are good and very stable, with the lowest RSME variance. The prediction results of GBDT have the lowest RMSE for the whole week, and the variance is the second-best only behind the RT model. As a result, the GBDT model is selected as the most suitable model for the passenger load factor prediction in this study due to the benefits which the GBDT model are brought including, 1) high prediction accuracy, 2) fast prediction speed while only requiring modest memory, 3) without requiring complex feature engineering to perform well, and 4) ability to handle a mixture of feature types.

#### 5.4 Comparison of Three Energy Management Strategies

In this subsection, the proposed method is evaluated and discussed with true passenger load data of Guangdong Transit Bus Line 11 on 12/15/2014 and CBDC. The real passenger load data at peak hour 8:00 AM and off-peak hour 12:00 PM are used in the test because the tests in these hours represent the most and least impacts of loading effect. The plot of true and GBDT predicted passenger load factors on this day are presented in Fig. 20. The predicted and true passenger load factor aligns very well over the 16 hours span without large error. The comparison results are summarized in Table 6. During the busy hours (i.e., 8:00 AM), the prediction error is under 10%. At noon, the error is large at 20% due to the low absolute load factor at around 30%.

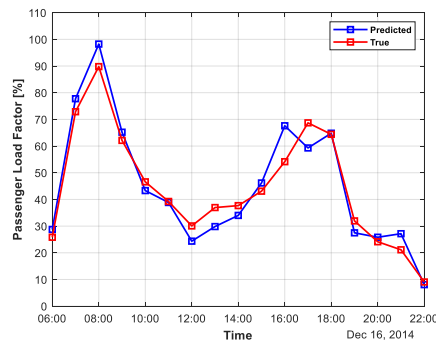


Figure. 20. Predicted and true passenger load factors of Guangdong city bus line 11 on 12/15/2014.



Table 6

Predicted and true passenger load factor, and prediction error at peak and off-peak hours of Guangdong city bus line 11 on 12/15/2014.

Hour	Predicted Load Factor	True Load Factor	Absolute error	Error percentage
8:00 AM	98%	90%	8%	8.9%
12:00 PM	24%	30%	6%	20%

In order to evaluate the performances of the proposed method, its test results are compared with the results of optimal DP strategies and the pure rule-based method, which does not consider the loading effect. The pure rule-based method used in the test is generated from the CBDC speed profile. However, under other driving cycles, the driving patterns that are different from the CBDC, the performance of the pure rule-based method may lead to significant downgrades. Thus, the rule-based method results in the test represent the best performances that a conventional rule-based method can bring for an electric city bus. The optimal DP strategies are generated from the true passenger load factors and actual speed profile and represent the best results that can be gained at these vehicle operating conditions.

The comparison results at 8:00 AM are shown in Fig. 21 and Table 7. These total costs of the proposed method, pure rule-based method, and optimal DP strategy are 3.6890, 4.1181, and 3.6885 USD, respectively. As shown in the supercapacitor SOC subplot, the proposed method provides a similar control strategy as the optimal DP strategy, while the pure rule-based method has a totally different SOC curve. Multiple supercapacitor SOC saturations are spotted between 400s and 1200s, which disables the possibility of discharge assistant to the battery at high power demand situations. This leads to the peaks from the pure rule-based method in the battery power subplot, during which the battery power sits at low levels for the other two methods. The proposed method and optimal DP method have a smoother battery SOC curve than the pure rule-based method. Even though the pure rule-based method shows the least cumulative cost at 450s, its supercapacitor SOC saturates at that time, and the cost immediately goes up, finally surpasses the costs from the other two methods. For the proposed method, even if there is an 8.9% prediction error of the passenger load factor, only 0.0136% of the difference between the total costs of the proposed method and the optimal DP strategy is introduced. On the other side, the proposed method brings 10.4199% of cost reduction than the pure rule-based method in the peak-hour.

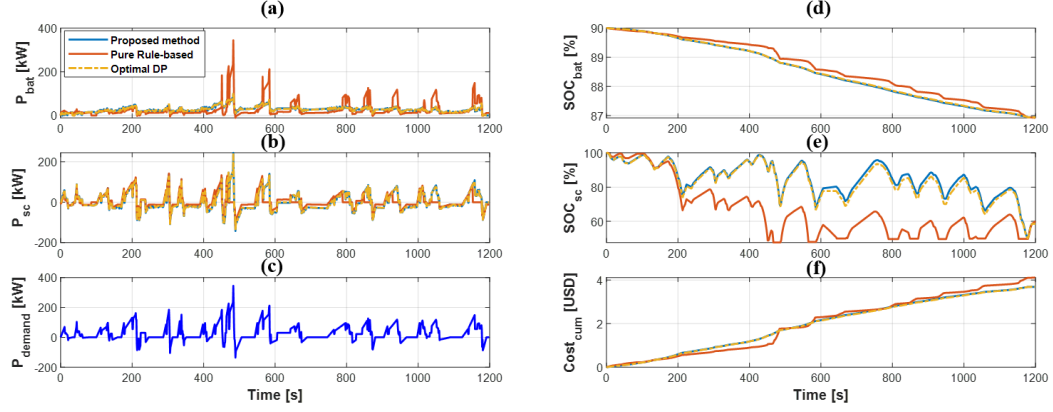


Figure. 21. Comparison of the proposed method, pure rule-based method, and optimal DP strategy with CBDC and true passenger load factor at 8:00 AM of Guangdong Transit Bus Line 11 on 12/15/2014: (a) power profiles of batteries, (b) power profiles of supercapacitors, (c) power demand profile, (d) SOC profiles of batteries, (e) SOC profiles of supercapacitors, and (f) total cumulated cost.

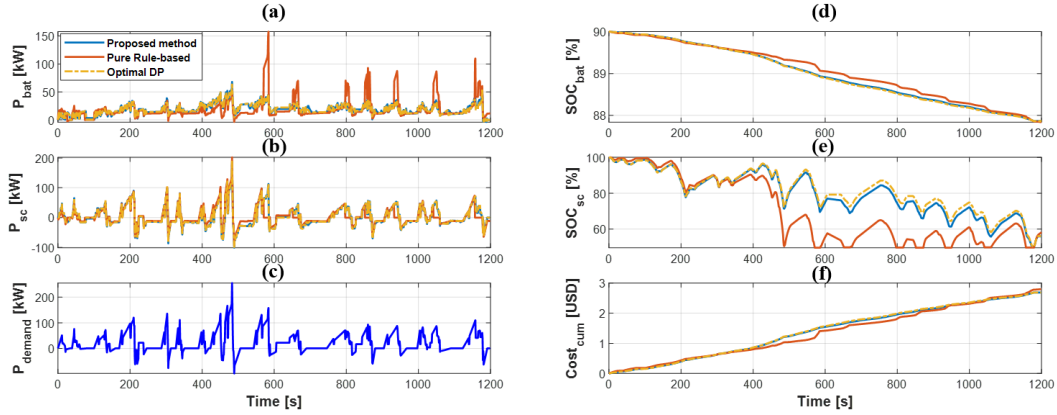


Figure. 22. Comparison of the proposed method, pure rule-based method, and optimal DP strategy with CBDC and true passenger load factor at 12:00 PM of Guangdong Transit Bus Line 11 on 12/15/2014: (a) power profiles of batteries, (b) power profiles of supercapacitors, (c) power demand profile, (d) SOC profiles of batteries, (e) SOC profiles of supercapacitors, and (f) total cumulated cost.

Table 7

Total costs of proposed and pure rule-based methods compare with the optimal DP cost at the peak hour (8:00 AM) and off-peak hour (12:00 PM).

Methods	Peak Hour (8:00 AM)		Off-peak Hour (12:00 PM)	
	Total Cost (USD)	Compare with Optimal DP	Total Cost (USD)	Compare with Optimal DP
Proposed method	3.6890	0.0136 % more cost	2.6869	0.0298 % more cost

Pure rule-based method	4.1181	11.647 % more cost	2.7973	4.1398 % more cost
------------------------	--------	--------------------	--------	--------------------

As shown as Fig. 22 and Table 7, the total cost of the proposed method, pure rule-based method, and optimal DP strategy at 12:00 PM are 2.6869, 2.7973, and 2.6861 USD, respectively. The proposed method has a very similar SOC trajectory of the supercapacitors as the optimal DP strategy. The difference in the total costs between the proposed method and the optimal DP strategy is 0.0298%, while a 25% error of the passenger load factor is introduced. It means that the proposed method is very robust against the prediction error of the passenger load factor. One thing remarkable is that, before the 1000s, the cost of the pure rule-based method is low than the costs of the proposed method and optimal DP. The reason is that with prediction and prior knowledge about the future power demand, the proposed method and rule-based method focus on minimizing the total cost of the whole circle rather than the current cost. Thus, using these two strategies, the batteries will charge and save the energy of supercapacitors for the future. It leads to higher costs at the beginning but saves more cost in the end because it allows the supercapacitors to have enough energy to supply during high power demands conditions. Besides, it further illustrates that without the predictions of future power demands, the performance of the traditional rule-based methods is limit. In addition, even if the 12:00 PM is the off-peak hour, which includes the less loading effect, the proposed method leads 3.946% of cost improvement than the pure rule-based method.

## 6. Conclusion:

In this paper, a dynamic programming approach is utilized as the battery/ supercapacitor hybrid electric bus EMS in the battery aging effect and passenger loading effect discussion. The passenger loading effect plays a more dominant role than the battery aging effect does on the bus operation cost. Four different models are presented for predicting the passenger load factors of city buses. GBDT Model is selected as the best passenger load factor prediction model for its high accuracy and stability. Even though the neural networks model has high accuracy in certain days, its performance is not consistent throughout the entire week, and its stability is extremely bad. A new EMS comprised of a cloud DP and rule-based controller with the rule update is proposed. To evaluate the proposed EMS performances, the proposed EMS is compared with the optimal DP method and the pure rule-based method. In this case, the proposed EMS and optimal DP share similar results with less than 1% difference. At peak and off-peak hours, the proposed EMS reduces 10.419% and 3.946% cost than the pure rule-based method.

In future studies, the size of the optimal components of supercapacitor and battery could be conducted. Besides, the performance of the rule-based controller used on the vehicle side can be further improved by increasing its rule with more heuristic principles in the EMS field.

#### Reference:

- [1] Cook, J., Oreskes, N., Doran, P.T., Anderegg, W.R.L., Verheggen, B., Maibach, E.W., Carlton, J.S., Lewandowsky, S., Skuce, A.G., Green, S.A., Nuccitelli, D., Jacobs, P., Richardson, M., Winkler, B., Painting, R., Rice, K., 2016. Consensus on consensus: a synthesis of consensus estimates on human-caused global warming. *Environ. Res. Lett.* 11, 048002. <https://doi.org/10.1088/1748-9326/11/4/048002>
- [2] Yang, F., Xie, Y., Deng, Y., Yuan, C., 2018. Predictive modeling of battery degradation and greenhouse gas emissions from U.S. state-level electric vehicle operation. *Nature Communications* 9, 2429. <https://doi.org/10.1038/s41467-018-04826-0>
- [3] Xu, B., Rathod, D., Zhang, D., Yebi, A., Zhang, X., Li, X., Filipi, Z., 2020. Parametric study on reinforcement learning optimized energy management strategy for a hybrid electric vehicle. *Applied Energy* 259, 114200. <https://doi.org/10.1016/j.apenergy.2019.114200>
- [4] Yan, S., Chi, C.-J., Tang, C.-H., 2006. Inter-city bus routing and timetable setting under stochastic demands. *Transportation Research Part A: Policy and Practice* 40, 572–586. <https://doi.org/10.1016/j.tra.2005.11.006>
- [5] Kivekäs, K., Lajunen, A., Vepsäläinen, J., Tammi, K., 2018. City Bus Powertrain Comparison: Driving Cycle Variation and Passenger Load Sensitivity Analysis. *Energies* 11, 1755. <https://doi.org/10.3390/en11071755>
- [6] Zhang, J., Lv, C., Qiu, M., Li, Y., Sun, D., 2013. Braking energy regeneration control of a fuel cell hybrid electric bus. *Energy Conversion and Management* 76, 1117–1124. <https://doi.org/10.1016/j.enconman.2013.09.003>
- [7] Pihlatie, M., Kukkonen, S., Halmeaho, T., Karvonen, V., Nylund, N.-O., 2014. Fully electric city buses - The viable option, in: 2014 IEEE International Electric Vehicle Conference (IEVC). Presented at the 2014 IEEE International Electric Vehicle Conference (IEVC), pp. 1–8. <https://doi.org/10.1109/IEVC.2014.7056145>
- [8] An, K., 2020. Battery electric bus infrastructure planning under demand uncertainty. *Transportation Research Part C: Emerging Technologies* 111, 572–587. <https://doi.org/10.1016/j.trc.2020.01.009>
- [9] Song, Z., Li, J., Han, X., Xu, L., Lu, L., Ouyang, M., Hofmann, H., 2014. Multi-objective optimization of a semi-active battery/supercapacitor energy storage system for electric vehicles. *Applied Energy* 135, 212–224. <https://doi.org/10.1016/j.apenergy.2014.06.087>
- [10] Hou, J., Sun, J., Hofmann, H., 2017. Battery/flywheel Hybrid Energy Storage to mitigate load fluctuations in electric ship propulsion systems, in: 2017 American Control Conference (ACC). Presented at the 2017 American Control Conference (ACC), pp. 1296–1301. <https://doi.org/10.23919/ACC.2017.7963131>

- [11] Liu, S., Wei, L., Wang, H., 2020. Review on reliability of supercapacitors in energy storage applications. *Applied Energy* 278, 115436. <https://doi.org/10.1016/j.apenergy.2020.115436>
- [12] Martinez, C.M., Hu, X., Cao, D., Velenis, E., Gao, B., Wellers, M., 2017. Energy Management in Plug-in Hybrid Electric Vehicles: Recent Progress and a Connected Vehicles Perspective. *IEEE Transactions on Vehicular Technology* 66, 4534–4549. <https://doi.org/10.1109/TVT.2016.2582721>
- [13] Xu, B., Hou, J., Shi, J., Li, H., Rathod, D., Wang, Z., Filipi, Z., 2020. Learning Time Reduction Using Warm Start Methods for a Reinforcement Learning Based Supervisory Control in Hybrid Electric Vehicle Applications. *IEEE Transactions on Transportation Electrification* 1–1. <https://doi.org/10.1109/TTE.2020.3019009>
- [14] López-Ibarra, J.A., Goitia-Zabaleta, N., Herrera, V.I., Gaztañaga, H., Camblong, H., 2020. Battery aging conscious intelligent energy management strategy and sensitivity analysis of the critical factors for plug-in hybrid electric buses. *eTransportation* 5, 100061. <https://doi.org/10.1016/j.etrans.2020.100061>
- [15] Xiong, W., Zhang, Y., Yin, C., 2009. Optimal energy management for a series–parallel hybrid electric bus. *Energy Conversion and Management* 50, 1730–1738. <https://doi.org/10.1016/j.enconman.2009.03.015>
- [16] Xie, S., Li, H., Xin, Z., Liu, T., Wei, L., 2017. A Pontryagin Minimum Principle-Based Adaptive Equivalent Consumption Minimum Strategy for a Plug-in Hybrid Electric Bus on a Fixed Route. *Energies* 10, 1379. <https://doi.org/10.3390/en10091379>
- [17] Sockeel, N., Shi, J., Shahverdi, M., Mazzola, M., 2018. Pareto Front Analysis of the Objective Function in Model Predictive Control Based Power Management System of a Plug-in Hybrid Electric Vehicle, in: 2018 IEEE Transportation Electrification Conference and Expo (ITEC). Presented at the 2018 IEEE Transportation Electrification Conference and Expo (ITEC), pp. 1–6. <https://doi.org/10.1109/ITEC.2018.8449957>
- [18] Song, Z., Hofmann, H., Li, J., Han, X., Ouyang, M., 2015. Optimization for a hybrid energy storage system in electric vehicles using dynamic programming approach. *Applied Energy* 139, 151–162. <https://doi.org/10.1016/j.apenergy.2014.11.020>
- [19] Time-Efficient Stochastic Model Predictive Energy Management for a Plug-In Hybrid Electric Bus With an Adaptive Reference State-of-Charge Advisory - IEEE Journals & Magazine [WWW Document], n.d. URL <https://ieeexplore.ieee.org/document/8270601> (accessed 10.13.20).
- [20] Moura, S.J., Fathy, H.K., Callaway, D.S., Stein, J.L., 2011. A Stochastic Optimal Control Approach for Power Management in Plug-In Hybrid Electric Vehicles. *IEEE Transactions on Control Systems Technology* 19, 545–555. <https://doi.org/10.1109/TCST.2010.2043736>
- [21] Zhang, F., Hu, X., Langari, R., Cao, D., 2019. Energy management strategies of connected HEVs and PHEVs: Recent progress and outlook. *Progress in Energy and Combustion Science* 73, 235–256. <https://doi.org/10.1016/j.pecs.2019.04.002>
- [22] Hou, J., Song, Z., 2020. A hierarchical energy management strategy for hybrid energy storage via vehicle-to-cloud connectivity. *Applied Energy* 257, 113900. <https://doi.org/10.1016/j.apenergy.2019.113900>

- [23] Xing, Y., Lv, C., Wang, H., Cao, D., Velenis, E., Wang, F.-Y., 2019. Driver Activity Recognition for Intelligent Vehicles: A Deep Learning Approach. *IEEE Transactions on Vehicular Technology* 68, 5379–5390. <https://doi.org/10.1109/TVT.2019.2908425>
- [24] Ma, Z., Xing, J., Mesbah, M., Ferreira, L., 2014. Predicting short-term bus passenger demand using a pattern hybrid approach. *Transportation Research Part C: Emerging Technologies* 39, 148–163. <https://doi.org/10.1016/j.trc.2013.12.008>
- [25] Mercedes-Benz Buses: eCitaro [WWW Document], n.d. URL [https://www.mercedes-benz-bus.com/en\\_DE/models/ecitaro.html](https://www.mercedes-benz-bus.com/en_DE/models/ecitaro.html) (accessed 10.13.20).
- [26] Song, Z., Hofmann, H., Li, J., Hou, J., Han, X., Ouyang, M., 2014. Energy management strategies comparison for electric vehicles with hybrid energy storage system. *Applied Energy* 134, 321–331. <https://doi.org/10.1016/j.apenergy.2014.08.035>
- [27] Zhang, L., Hu, X., Wang, Z., Sun, F., Dorrell, D.G., 2018. A review of supercapacitor modeling, estimation, and applications: A control/management perspective. *Renewable and Sustainable Energy Reviews* 81, 1868–1878. <https://doi.org/10.1016/j.rser.2017.05.283>
- [28] Schmidhuber, J., 2015. Deep Learning in Neural Networks: An Overview. *Neural Networks* 61, 85–117. <https://doi.org/10.1016/j.neunet.2014.09.003>
- [29] Loh, W.-Y., 2011. Classification and regression trees. *WIREs Data Mining and Knowledge Discovery* 1, 14–23. <https://doi.org/10.1002/widm.8>
- [30] Friedman, J.H., 2001. Greedy function approximation: A gradient boosting machine. *Ann. Statist.* 29, 1189–1232. <https://doi.org/10.1214/aos/1013203451>
- [31] Bellman, R., 1966. Dynamic Programming. *Science* 153, 34–37. <https://doi.org/10.1126/science.153.3731.34>